Journal of Materials Chemistry C

Accepted Manuscript

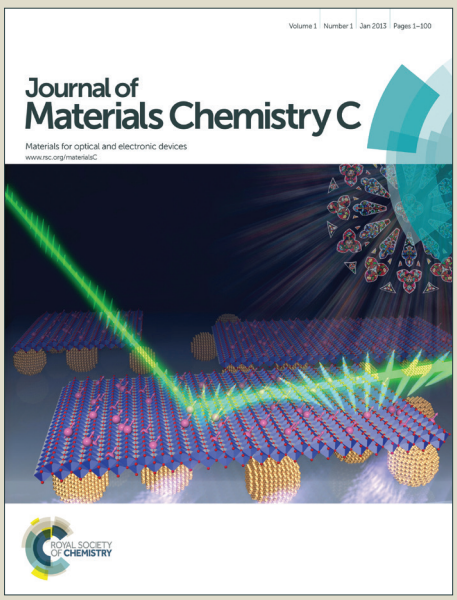

ROYAL SOCIETY OF CHEMISTRY

www.rsc.org/materialsC

Design, synthesis and application of hydrogen bonded smectic liquid crystals matrix encapsulated ZnO nanospikes

Kaushik Pal[†], **MLN Madhu Mohan**[‡], **Bihong Zhan**[†] and **Guoping Wang**[*]

[†,*] *School of Power and Mechanical Engineering, Wuhan University, 8 East Lake South Road, Wuhan 430072, China.*

[‡]*Liquid Crystal Research Laboratory (LCRL), Bannari Amman Institute of Technology Sathyamangalam 638 401, India.*

*Corresponding author:

Guoping Wang (guopingwang@whu.edu.cn); **Tel:** (+86) 136 1863 4882

Abstract

Efficient ZnO nanospikes, due to their novel properties, are promising components in a wide range of nanoscale devices for future applications. Herein, current research activities are focused on the synthesis, characterization and applications of ZnO nanostructures encapsulated hydrogen bonded liquid crystal matrix (HBLC e.g. azelaic acid and heptyloxy benzoic acid) optical switching. We briefly describe the smartest applied methodologies for the synthesis of ZnO nanostructures and smooth dispersion under liquid crystalline optical materials. In fact, recently HBLCs doping was found significant influence on the nucleation and growth of many functional nanocrystals (NCs), and provide a fundamental approach to modify the crystallographic phase, size, morphology, and electronic configuration of nanomaterials. All the homologies of the present series show rich mesomorphism exhibiting orthogonal and tilted phases. A range of remarkable characteristics is then presented, organized into sections describing the optical, electrical and electro-optical phase transition and DC bi-stable switching properties. The other display parameters such as spontaneous polarization, rotational viscosity, switching response, capacitance, dielectric permittivity, dielectric loss spectra and low frequency relaxation (Gold stone mode) are also investigated in these nanospikes-HBLC composite and found quite convincing to the described observations in this article. Moreover, polarizing optical microscopy revealed various phases in different textural appearance that proof the influence of the nanomaterial. Most observed phenomena are discussed in terms of a new smectic ordering labeled as smectic X*, which is sandwiched between traditional nematic and convectional smectic C* phases. Dielectric relaxations in the smectic C* phase of pure and doped LCs have been analyzed. In this feature article, we provide an overview of the most recent progresses in HBLC (AC+7BAO) doping-induced control of efficient switching, as well as high performances of novel functional nanomaterials for the first time. These investigations are developing versatile applications of Opto-electronic and high resolution liquid crystal devices.

Key Words: Nanospikes, Liquid Crystals, Dielectric relaxations, smectic X*, optical switching

1. Introduction.

The unique and fascinating properties of nano-structured materials have triggered tremendous motivation compared with their bulk equivalents, among scientists to explore the possibilities of using them in industrial and technological appliances. Coupled with their small size, which is of relevance to technology's increased demand for continuing to ever expand interest in liquid crystalline materials. Zinc oxide is a versatile semiconductor material with a wide band gap of 3.3 eV at RT, which has been found useful in many applications such as opto-electronic devices, surface acoustic wave devices, field emitters, piezoelectric devices, transparent conducting materials and solar cells.[1-10]

Dispersed liquid crystal composite materials have received significant attention by research community due to their potential application in electro-optic displays.[11, 12] Immense work was done on dispersed liquid crystal materials doped with polymers and dyes to understand the liquid crystal behavior and improve the physical, electro-optical and electrical properties of existing liquid crystals (LCs).[13, 14] Among dispersed LC systems, nanomaterials such as zinc oxide nanospikes doped thermo tropic liquid crystals systems have shown tremendous interest due to the unique thermal, mechanical, and electrical properties of nanospikes.

In particular, one-dimensional (1D) ZnO nanospikes represent an extremely novel class of nanomaterials, as demonstrated by the rapidly expanding literature concerning their synthesis, dispersion under liquid crystals for remarkable fast switching response and characterization. On the other hand, ZnO is attracting considerable attention due to its unique ability to form a variety of nanostructures such as nanowires, nanoribbons, nanobelts, nanocombs, nanorings, nanocages, nanocastle, nanospheres, nanofibers, nano-tetrapods and heterostructures.[15-16]

Recently, keeping in pace with topical science, liquid crystals have entered into the fascinating domains of Nanoscience and Nanotechnology. Fundamentally, liquid crystals exhibiting the intermediate phases during their phase transitions have both the properties of conventional solid and isotropic liquid which makes these unique systems and gives rise to many interesting properties leading to the engineering application aspects.[17-18] Molecular orientation and the self-assembly systems from the basic requirements for exhibiting these interesting properties. Hydrogen bonding is one of the principal intermolecular forces which helps in the construction of such supra molecular structures and is the key interactions for the chemical and biological processes in nature. [19–27] This core work deals with nanomaterials involves homologous series of hydrogen bonded liquid crystals (HBLC) formed between azelaic acid and p-n-heptyloxy benzoic acids (Nubia) referred as 'AC+nBAO', where carbon number n=7 and m=7 for AC as shown chemical structure in Fig1a and also Fig1b diagrammatically shown HBLC structure. Furthermore, since the liquid-crystal medium responds to small external stimuli, the dispersed materials can be forced to follow the order of the host medium which elaborates the controlled dynamic self-assembly and (re) orientations of the dispersed nanomaterials. A specific, present study is dedicated to focus on the dispersion of 1-D ZnO nanospikes dispersed in HBLC as a colloidal suspension, with the aim of showing their effects on the electro-optical properties and dynamical response. The influence of the nanospikes dopant concentration on the electro-optical, material and dielectric parameters has been evaluated comparable with pure LCs.

Additionally, we are fond of our device fabrication according to standard techniques, which actually consists of two counter indium tin oxide (ITO) coated glass substrates with a rubbed Polyimide (PI) alignment layer. First, we dropped the suspension solution of ZnO nanospikes onto the rubbed PI layer until nanospikes were dried. After the combination of top and bottom

treated substrates in the same rubbed direction, hydrogen bonded liquid crystals from Sigma Aldrich was injected into the assembled substrates. A supersonic treatment was employed to obtain a better mixture of the HBLC molecules and ZnO nanospikes. Further detailed investigation of sample preparation and distribution mechanism into the ITO cell device confined geometry can be represented by the schematic diagram as follows in Fig 2.

The test device for dynamic measurements were prepared using 0.7 mm ITO-coated polished glass plates having 16 (4mm X 4mm) conducting coating imprinted on the ITO coating by photolithography which is referred as a pixel. Polymer coated film on ITO cells rubbed unidirectional and perpendicular to applied electric field. The thickness of the cells was about 10 μm, thin enough to allow surface stabilization of the specimen. Slices mounted on the glass sheet on opposite sides of the hole served as electrodes. They are provided with the driving electric fields in the film plane. We studied the images of the films with a reflection microscope. Fig 3 shows a schematic of the side-view structure of the LC cell with and without an external electric field.

Moreover, we have observed the change in the nature of dielectric anisotropy with changing the electro-optical parameters. We have used ZnO nanospikes, which provided best alignment of thermo tropic LC molecules in our cells. The switching behavior of LC molecules has been affected due to the presence of nanospikes in the pure LC system. The temperature dependence of the other display parameters such as: spontaneous polarization, rotational viscosity, electro-optical switching response, dielectric anisotropy, threshold voltage, bi-stable DC switching and low frequency relaxation (Gold stone mode) has also been discussed with the help of different attempts of various nanomaterials and LCs and hybrid mixture[28-33] and also investigated in these nanospikes-HBLC composite and found quite convincing to the described observations in this

article. HBLC involves the intentional incorporation of atoms or ions of suitable elements into host lattices is one of the effective routes to endow electronic and optical properties, enhancement of switching response, liquid-crystalline phase behavior of nanomaterials themselves, self-assembly and alignment of nanomaterials in liquid-crystalline media, and the synthesis of nanomaterials by using liquid crystals as 'templates' or 'precursors' have been covered up whole theme.

2. Experimental details

2.1 Synthesis of ZnO nanomaterials

All the chemical reagents used in this experiment were of analytical grade and used without further purification. The novel hydrothermal method is employed for the synthesis of nanostructures.

Both elemental and compounds nanostructures can be obtained via this method by choosing appropriate starting materials and suitable reaction conditions. In brief, 3 mmol of a zinc acetate dehydrate [$Zn(CH_3COO)_2.5H_2O$] mixed under strong, vigorous stirring into 5 mmol alkaline media (5M of NaOH and 3M KOH).

Complete stirred for 30 min, a homogeneous milk type solution formed and then transferred into a 100 ml Teflon-lined stainless-steel coated autoclave. The autoclave was sealed and maintained at 120°C for 2.3 hours, and then air-cooled to room temperature. The dark gray precipitates were collected and washed with ethanol (twice) and deionized distilled water (several times). The desired powder like samples was allowed to dry with a flow of Nitrogen (N_2) gas. Thus, ZnO nanospikes were obtained for further spectroscopic characterization.

2.2 Preparation of liquid crystal samples

Hydrogen bonded liquid crystals is composed of p-n-heptyloxy benzoic acids *n*BAO with azelaic acid supplied by Sigma Aldrich, (Germany). Intermolecular double hydrogen bonded mesogens

were synthesized by the addition of two moles of p-n-alkoxybenzoic acids (nOBA) with one mole of azelaic dicarboxlic acid into N,N-Dimethyl formamide (DMF). Further, they were taken subject to constant stirring for 12 hours at ambient temperature (45^{o}C) till a white precipitate in a dense solution is formed. The white crystalline crude complexes were obtained by removing excess DMF are recrystallized with dimethyl sulfoxide (DMSO) and the yield varied from 75% to 99%. The formation of multimer is avoided by recrystallization of the product. The detail of the chemical reaction process of liquid crystals crystallization was shown in Fig 1a.

2.3 Preparation of Nanomaterials dispersed Liquid Crystals (NDLC)

Typical amounts (0.35 gm) of as-synthesized ZnO nanospikes were combined with 0.005% as-prepared pure liquid crystals suspension. The solution was vigorously stirred during 1 hour, followed by ultrasound vibration for complete dispersion. After that, the deposition was collected and vacuum dried at 50°C for 2 hours, which has the function of facilitating the combination of the ZnO nanospikes with the liquid crystals.

Commercial electro-optical cells with ITO electrodes (electrode area 4×4mm^2) and alignment layers were deposited on the inner surface of the confining substrates; the alignment layers were rubbed in unidirectional and assembled in an antiparallel fashion with respect to the rubbing directions for a planar alignment. The cell gap was maintained with 2 μm spacer placed between the substrates. This free cell is placed into hot plate under treatment of (5°C/min). NDLCs samples were distributed inside heated cells by flow of capillary action. Suspensions fabricated in this way were then put into photorefractive liquid crystal cells. The sample preparation techniques and smooth distribution inside cell by capillary action were represented by the schematic diagram in Fig 2.

2.4 Sample characterizations

The crystal morphology and structures of the resulting products grown on SiO_2 substrates and characterized by Field Emission Scanning Electron Microscopy (Model: SIGMA ZEISS FE-SEM) using a JEOL electron microscope 6700 equipped with a field emission gun operating at 3kV. Chemical composition detection observed by energy dispersion spectroscopy (Model: EDAX GENSIS, 200 V-30 kV, AMETEK, USA).

The frequency dispersion dielectric data were recorded at room temperature at frequencies ranging from 10 Hz to 20 MHz using (Model: Microtest-6620) low frequency Impedance Analyzer. The thickness of the photo refractive test cells was about 0.1μm, thin enough to allow surface stabilization of the specimen. Frequency dependent complex dielectric permittivity ε*(ω) is determined using the following equation [34-35]:

$$\boldsymbol{\varepsilon^*(\omega)} = \frac{1}{j\omega C_0 Z^*(\omega)} = \frac{C_P}{C_0} - j\,\frac{1}{\omega C_0 R_P} = \boldsymbol{\varepsilon^{/} - i\varepsilon^{//}} \qquad (1)$$

Where $\varepsilon^{/}$ is the dielectric constant and $\varepsilon^{//}$ is the dielectric loss. Where *j* denotes the square root of -1, ω (=2Π*f),* is the angular frequency, *Z* stands for the complex impedance, C_0 and Cp are the capacitance of the cell under the vacuum and that filled with a dielectric bulk, respectively, Rp is the effective parallel resistance of the dielectric cell (consisting of a planar LC bulk in this study), and $\boldsymbol{\varepsilon^{/}}$ and $\boldsymbol{\varepsilon^{//}}$ represent the real and imaginary parts of the complex dielectric constant, respectively.

Surface stabilized smectic uniform lying helical texture and electro-optical switching with different temperature variation calculated by polarizing optical microscopy (Model: OLYMPUS, CX31, 6J09934 Japan) with a signal generator U8031A. The spontaneous polarization (P_s) and

the relaxation time were measured by using a polarization reversal method equation (1) and calculated with the help of the following relation[18, 36-37]:

$$P_s = (\frac{1}{2A})\int i(t)dt \qquad (2)$$

All associated measurements were based on graphical computation, which follows equation (2). The viscosity (γ) was determined from the measured value of the spontaneous polarization (P_s) and the switching response time (τ) using the following relation[18];

$$\tau = \frac{\gamma}{1.75 P_S E} \qquad (3)$$

Smectic X phase liquid crystals (azelaic acid with p-n heptyloxy benzoic acids) were prepared by evacuating the liquid crystal using the appropriate solvent. This liquid-crystalline molecule is also composed of rigid and flexible parts and corresponding phase sequence given below;

HBLC (AC+7BAO): Crystal (66.9°C) ↔ (71.5°C) Smectic C* ↔ (81.9°C) Smectic X* ↔ (113.2°C) Nematic ↔ (113.5°C) Isotropic

Bi-stable DC switches I~V response measurement through the digital source meter (Model: Agilent 33522A, 30 MHz function/Arbitrary waveform generator).

3. Results and discussions

3.1 Structure and morphology

Tailoring growth dynamics of the structural morphology of the as-prepared product was observed by FE-SEM investigation at different magnifications was shown in Fig 4 (a-c). Macroscopically, as shown in Fig 4a, it is apparent that the nanospikes structures evolved and comprising with average diameter ≈ 85.7 nm and large distribution of length ≈ 1.62 μm. The typical surface morphology of the ZnO nanospikes also can be clearly observed in Fig 4b, while high magnification observed in Fig 4c. Additionally, hydrogen bonded liquid crystallographic 'worm' like features appeared in Fig 4d.

To further investigate the distribution of chemical elements by Energy Dispersion Spectroscopy (EDS) pattern indicating an atomic ratio of K-shell electron orbital e.g. Zinc and oxide of 24.63 to 18.34 for ZnO nanospikes composed of others liquid crystal elements. It was corresponds to Fig 5, which identifies the high purity of as-preparative LC dispersed ZnO nanomaterials.

3.2 Optical Characterization

The ZnO nanostructures were analyzed by X-ray photo- electron spectroscopy (XPS; Model: Thermo Fisher COMPANY ESCALAB 250Xi Photoelectron spectrometer). Fig 6 illustrated the typical XPS wide survey spectra of various morphologies of ZnO nanospikes. Zn, O and C peaks were detected as shown in the three wide survey spectra. The detected carbon is related to the carbon adsorbed on the surface during the exposure of the sample to the ambient atmosphere. This also demonstrated the comparison of raw data of high resolution XPS spectra of the Zn 2p region (I) and O 1s core-level (II) of various morphologies of ZnO nanospikes. The Zn 2p core-level of ZnO NS has two fitting peaks located at about 1022 and 1044 ev attributed to $ZnP_{1/2}$ and Zn $P_{3/2}$, respectively. Similarly, those two fitting peaks located at 1018 and 1042 ev are attributed to Zn $P_{1/2}$ and Zn $P_{3/2}$ of ZnO nanospikes respectively. These results indicate that the chemical valance of Zn at the surface of nanospikes (+2 oxidation state). Zn $2P_{3/2}$ peak was fitted to only one Gaussian in all samples analyzed. The binding energy difference between the $ZnP_{1/2}$ and Zn $P_{3/2}$ is 13eV corresponding to nanospikes morphology.

Interferometer offers high sensitivity for optical imaging by providing information about the complex electric field. Using interferometer (Model: 02TV003, VD-IIA DPSS LASER DRIVER, sn: 011301) allows for measurements in changes of field amplitude which can reveal the presence of nanospikes dispersed liquid crystals via their absorptive or scattering properties. However, the complex field can also be measured to determine a scattering phase shift due to the

presence of nanospikes encapsulated liquid crystals depicted in Fig 7a, while the inherent phase shift due to the plasmon resonance can thus be used to detect nanospikes and liquid crystalline molecules. Additionally, the scattering phase shift can be further enhanced by using a localized heating to intentionally vary the local phase as is done in the photo thermal approach and pattern diagram shown in Fig 7b.

3.3 Electrical and Optical switching Response Characteristics

The variation of relaxation frequency with temperature for (AC+7BAO) in Gold stone mode of smectic C* phase has been done at five temperatures, namely 81.9^{o}C, 79.1^{o}C, 77.1^{o}C, 71.5^{o}C and 70.1^{o}C covering the entire thermal span of smectic C* to smectic X* phase. The data obtained is plotted in Fig 8a, with permittivity on x-axis and dielectric loss on y-axis. It can be observed from the figure that as the temperature decreases the magnitude of the relaxation frequencies decreases and shifts to lower side which is in accordance with the reported data on ferroelectric liquid crystals. Hence, in Gold stone model of smectic C* phase of pure LC (AC+7BAO) the suppression of the dielectric relaxation at various applied fields has been recorded. In fact the suppression of dielectric relaxation with applied field has been noticed in the entire thermal span of smectic C* phase. At five various applied fields, namely 0 V/μ, 2V/μ, 4V/μ, 6V/μ and 8V/μ the dielectric loss magnitude with permittivity is recorded at 71.5^{o}C and depicted in Fig 8b. The obtained data is plotted in Fig 8b with permittivity on x-axis and dielectric loss on y-axis. It can be observed from the figure that as the field increases the magnitude of the relaxation frequency decreases and gets suppressed which substantially proves the relaxation to be Gold stone model. The Cole-Davidson plot for one temperature (71.5^{o}C) as a representative case herein is shown below in Fig 8c. In fact it is distorted semicircle indicating a Cole-Davidson relaxation process. For all the other temperatures also it noticed that the dielectric relaxation follows Cole-Davidson

process. Subsequently, we investigated comparable study of temperature dependence frequency dispersion dielectric characteristics correspond to Zno-nanospikes dispersed LC sample. We have neglected the contribution in the air capacitance value from the alignment layer since it is very small. Temperature dependence complex dielectric permittivity ($\varepsilon^{/}$) and dielectric loss ($\varepsilon^{//}$) are plotted along y-axis vs. frequency along x-axis, is shown in Fig 9 (a) and (b) respectively. From critical analysis, Fig 9a the permittivity remains constant and certainly falls down at high frequency range, while peak intensity depends up to temperature variation from 30°C, 40°C, and 50°C. It only shows normal dispersion in the system from 6 kHz to 10,000 kHz. However, in case of dielectric loss spectra investigation, clear and prominent peaks are identified at same temperature variation from 30^{o}C to 50^{o}C depicted by dotted arrow (Fig 9b). So a high frequency relaxation and a low frequency relaxation are observed in the system that also confirmed by dielectric constant variation having two steps. Such relaxations may be occurred due to the inherent dipole moment of nanospikes interacting antiparallelly with the surrounding dipolar species to reduce the overall spontaneous polarization of the composite system.

3.4 FTIR-NMR study and Phase Identification

Typical FTIR spectra of hydrogen bonded liquid crystals (AC+7BAO) as shown in Fig. 10a. Infrared spectra of free p-n-alkoxybenzoic acid, azelaic acid and their intermolecular H-bonded complexes are recorded in the solid state (KBr) at room temperature. As a representative case, Fig 10a illustrates the FTIR spectra of the hydrogen bonded complex (AC+7BAO) in solid state at room temperature (31^{o}C). The solid state spectra of free alkoxy benzoic acid is reported [38] to have two sharp bands at 1685 cm^{-1}and1695 cm^{-1} due to the frequency ν(C=O) mode. The doubling feature of this symmetrical stretching mode confirms the dimeric nature of alkoxy benzoic acid at room temperature [38]. The absorption peak at 3106 cm^{-1} is due to the C-H

stretching of the aromatic systems. The absorption at 1427 cm^{-1} is attributed to the O-H in plane bending coupled with C-O stretching vibrations. In (AC+7BAO), the O-H stretching absorption band appeared at 2924 cm^{-1}. The presence of H-bonding in the present complexes is further inferred from the appearance of new band diagnostic of ν(O-H) at 2561 cm^{-1}. The doubling nature of ν(C=O) mode may be attributed to the dimeric nature of the acid group at room temperature [38] Corresponding spectrum of the solution state (chloroform) shows a strong intense band suggesting the existence of a monomeric form of benzoic acid. A noteworthy feature in the spectra of (AC+7BAO) series is that the appearance of a broad band at 1690 cm^{-1} and non appearance of the doubling nature of ν(C=O) mode of benzoic acid moiety. This clearly suggests that the dimeric nature of the benzoic acid dissociates and prefers to exist in a monomeric form upon complexation. Thus, through FTIR studies the hydrogen bond formation in both the above series has been evinced. Moreover, the proposed structure of (AC+nBAO) HBLC complexes has been verified by ^{1}H NMR studies. As a representative case ^{1}H NMR for AC+7BAO complex is discussed. The complexes are analyzed using Nuclear magnetic resonance spectroscopy (NMR; Model: Brucker international model ULTRA SHIELD of 300 MHz). The NMR spectrum of the complex is recorded in $CDCl_3$ with TMS as the internal standard. The recorded spectrum is shown in Fig 10b and the following chemical shifts were observed.

a) Broad resonance signals are observed approximately in the range of 0.5 – 2.8 ppm for methylene group. In (AC+7OBAO) complex these signals are observed between 2.969 - 0.793 ppm which are attributed [39] to the existence of backbone methylene.

b) Two sets of multiples between 6.848 -7.011ppm and 7.968 - 8.132 ppm are equivalent to 2H and attributed [39] to aromatic protons.

c) The existence of the methoxy proton unit resonance shows signal between 3.933 - 4.043 ppm. The proposed structure of the complex has been confirmed Fig 9b, the NMR study.

So far, the experimental characterizations have been carried out by commercial electro-optical cells with ITO electrodes sandwiched and cell gap was maintained with 2 μm spacer placed between two conducting substrates. Surface stabilized smectic uniform lying helical texture and electro-optical switching with different temperature variation calculated by polarizing optical microscopy (POM) with a signal generator employed voltage 5V.Hence, detailed texture analysis corresponding transition temperature of pure HBLC and ZnO nano-spikes doped liquid crystals observed under cross polarizer. Molecular alignment and uniform textures were slowly developed as the LCs isotropic temperature is cooled to room temperature. Also a small bias field is maintained to prevent cells for electro-optical switching. The phase transition of FLC (AC+7BAO) and nanospikes dispersed HBLC investigated three individual phase e.g. nematic (N), smectic C* and smectic X* phase with its transition temperature. Phase variance and texture patterns with the planar boundary conditions study through POM ensures from crystal structure corresponding at temperature as shown in Figs 11 and 12, while pure LC first heated until reached in its isotropic temperature (113.5°C) and cooled down slowly due to perfect alignment of molecules. The mesogens of the azelaic acid (AC) with p-n-heptyloxy benzoic acid (7BAO) with referred as (AC+7BAO) Fig 11, homologous series are found to exhibit characteristic textures viz., nematic (N) phase of droplet texture appeared at 113.2°C (Plate 1), threaded nematic schlieren texture (Plate 2), smectic C* (Sm C*) phase were identified with broken focal conic texture at 71.5°C (Plate 3), worm like textural appearance due to smectic X* phase (Sm X*) observed between phases Sm C* and N, at 81.9°C (Plate 4). Diagrammatic description of the phase variance of the pure HBLC mentioned above. Indeed, the texture pattern surprisingly

varied with applied temperature and small bias by introducing ZnO nanospikes induced HBLC illustrated in Fig 12. Different phase appeared due to earlier fashion temperature transition viz., the droplet texture of a nematic phase (N) appeared at 113°C (Plate1), threaded nematic oily texture (Plate2), mosaic texture pattern appeared at 71.2°C (Plate 3) due to Sm C* phase and new Sm X* phase investigated at 81°C with cumulate texture pattern (Plate 4) identified due to crystal phase. Thus, texture study from polarizing optical microscopy ensures that the transition temperature of nanospikes-HBLC mixture phase sequence (Crystal 66.2 Sm C* 71.2 Sm X* 81 N 113 Iso 112.9) is reduced than pure LC samples, resulted low response time with high switching rates established first in this article. This usually happens when micro- or nano-sized guest particles are present in the liquid crystal host. But more or less nanomaterials did not disturb the molecular orientation of the LC molecules.

Fig 13a, indicates the electrical response time (τ) plot against the applied electric field (E) at 30°C. The response time is reduced rapidly and exponentially in ZnO nanospikes dispersed LC cell while slowly reduces in the pure LC sample system. Actually nanospikes have a rich π-electron density along their tubular axis and also a very high aspect ratio. The possible π-electron electron stacking between LC molecules and nanospikes forms an electrical double layer (EDL). Again, due to the inherent dipole moment of the nanospikes an electric field is generated which interacts with those of the hydrogen bonded LC molecules. As a consequence of this interaction, a higher internal electric field is generated giving a faster response time.

The field and temperature variance of spontaneous polarization (P_S) through sample switching evidence as performed by a digital oscilloscope (Model: GW INSTEK, GDS-2302A equipped with triple output DC power supply KEYSIGHT U8031A, 0-30V,6A/5V,3A) as shown in Fig 13b. Spontaneous polarization attains a saturated value at the low temperature region; while near

the transition point of temperature at 71°C to 81.5°C drastically increase correspond to nanospikes dispersed LC, while it follows similar fashion quite shift peak intensity observed due to pure LC. It reveals the existences of Sm C* and Sm X* phases are ferroelectric phases. The suppression of the frequency with filed in both these phases have been noticed in pure LC samples. The formation of EDL around the nanospikes screens the polarization director of the doped LC sample, which is one of the possible reasons behind the molecular movement describing P_s. We also found that the spontaneous polarizations of all the two dipole species are almost the same in the LC cell, whereas for the pure sample four dipolar species possess a large spontaneous polarization. This P_s is related with phase transition points as following equation (4);

$$P_s(T) \propto (T - T_C)^{\beta} \qquad (4)$$

Where, T_c represents the transition temperature from isotropic to Smectic C*,β is the critical exponent component value. T is the temperature at which P_s (T) is experimentally determined. Additionally the field dependence of the optical tilt angle characteristic is depicted in Fig 13c. Applied lower field region the tilt angles smoothly falls in both occasions. No such remarkable response behavior noticed in the value for pure and doped cell. The optical tilt angle has been experimentally measured by optical extinction method[40] in smectic C* phase for all the members of nanospikes doped and pure LC (AC+7BAO) homologous series. Inset of Fig 13c depicts such variation of optical tilt angle with temperature and observed that the tilt angle increases with difference of transition temperature and attains maximum peak value of tilt angle are observed to be 25° and 22.8° correspond to ZnO-nanospikes dispersed LC and pure LC (AC+7BAO) cells respectively due to the signature of phase transition. These maximum magnitudes of the tilt angle are owed to the direction of the soft covalent hydrogen bond interaction that spreads along molecular long axis with finite inclination.

Interestingly, the behavior of the rotational viscosity shows similar characteristics to the polarization and its value lies between 250 and 3000 mN s m^{-2} (Fig 13d). With the increase of temperature from 66.9°C to the transition point we confirmed and detail investigation shows that the rotation viscosity rapidly increases with a transition temperature significantly due to the increase of degrees of freedom of LC doped with ZnO nanospikes. Also the relaxation frequency is higher in the nanospikes doped LC cell due to the increase in the rotational viscosity. At room temperature the nanomaterial in the LC matrix is frozen because of the strong confinement (LC interactions become stronger) of the LC matrix. This confinement is increased due to the thermal energy and the rotational mobility of the nanomaterial is increased. Precisely, conventional pure LC cell and a NDLC cell constructed with the doped nanospikes sandwiched two ITO cells Fig 14a, more magnificently represented in Fig 14b and the direction of polarization of HBLC molecules under cross polarizer schematically shown in Fig 14c. Microscopic investigation of the nanospikes NDLC composite on the surface mechanism responsible for the high resolution switching performance (‘On state’ and ‘Off sate’) with external bias field dependence under cross polarizer clearly depicted in Fig 14d.

The light transmittance of pure LC and ZnO nanospikes (NS) dispersed LC modules was measured as a function of the applied voltage at 20 Hz. Threshold less, hysteresis free U- shape switching is observed for both the occasions at temperature 70°C, as depicted in Fig 15. The voltage required for switching between two electrode systems is almost half of the doped cell revealing the enhanced sensitivity of the LC molecules to the applied electric field in the doped system. However, we believe that a cell of thickness less than the pitch of hydrogen bonded liquid crystal modules could have given a perfect surface-stabilized state and hence better switching. Applying a triangular wave voltage of 10 V and frequency 20 Hz, we measured the

contrast ratio (maximum transmission/minimum transmission) which turned out to be the same (1.5) for both the pure LC and ZnO nanospikes doped LCs cells.

Temperature dependence bi-stable DC switching of I~V response characteristics as illustrated in Fig 16. Adjusting different set of temperatures e.g. 40°C, 50°C, 60°C and 70°C the bias voltage increases correspondingly but current almost a similar randomly fashion due to nanospikes doped LCs, while no significant behavior was identified for LC itself. However, the LC materials, respond quite differently at threshold voltage region shows a conductor to insulator and again insulator to conductor type materials behavior indicated by a dotted arrow shown in room temperature. Thus the carrier concentration becomes higher and increasing the conductance.

4. Conclusions and outlook

Nanomaterials embedded liquid-crystal is a young emerging field of liquid crystal research and has received increasing attention over recent years. Liquid-crystalline nanomaterials have been successfully designed and investigated, in addition to synthesis and self-assembly of nanospikes in the liquid-crystalline medium itself. The influence of ZnO nanospikes into smectic liquid crystals (azelaic acid with p-n-heptyloxy benzoic acids *n*BAO) have resulted in striking differences in the dielectric and electro-optical behaviors. Based on frequency dispersion dielectric investigation, we can conclude that the field increases the magnitude of the relaxation frequency decreases and gets suppressed which substantially proves the relaxation to be Gold stone mode. The distorted semicircle indicating at temperature 71.5°C correspond to the Cole-Davidson relaxation process of homologous series (AC+7BAO) liquid crystals. Corresponding to I~V response curve bi-stable DC switching appeared (Conductor ↔ Insulator), so the fluctuation/stability of current also observed due to LC only. Whereas, some nanomaterials e.g. nanospikes have enjoyed the golden opportunity in LC Nanoscience so far, but better

opportunities may be in store for other nanostructures which can only be realized as the field moves forward and makes more significant advances. The special chemical structure can lead to the formation of new Sm X* phase appeared with temperature transition due to hydrogen bonded liquid crystals. A new smectic ordering labeled as Sm X* which is sandwiched between traditional nematic (N) and convectional Sm C* phases reveals a remarkable investigation. Moreover, the temperature at which the N phase observed, which is close to isotropic temperature, which is beneficial for fictionalizations. Within smaller than millisecond response time of the nanospikes dispersed LC is low compared to pure LCs, also a rapid response of rotational viscosity under smooth distribution explores promising applications in high contrast ratio of display device's technology.

Acknowledgements

This work was financially supported by the National Natural Science Foundation of China (Project grant No.61405148) and start-up of Wuhan University. Dr. Kaushik Pal is grateful to the above financial support for his postdoctoral study.

Notes and references:

1 M. H. Huang, S. Mao, H. Feick, H. Q. Yan, Y. Y. Wu, H. Kind, E. Weber, R. Russo and P. D. Yang, *Science*, 2001, **292**, 1897.

2 T. Aoki, Y. Hatanaka and D. C. Look, *Appl. Phys. Lett.*, 2000, **76**, 3257.

3 A. Bousfia, E. H. El Boudouti, D. Bria, A. Nougaoui, B. Djafan- Rouhani and V. R. Velasco, *J. Appl. Phys.*, 2000, **87**, 4507.

4 C. J. Lee, T. J. Lee, S. C. Lyu, Y. Zhang, H. Ruh and H. J. Lee, *Appl. Phys. Lett.*, 2002, **81**, 3648.

5 G. Sberveglieri, S. Groppelli, P. Nelli, A. Tintinelli and G. Giunta, *Sens. Actuators, B*, 1995, **25**, 588.

6 D. S. Ginley and C. Bright, *Mater. Res. Soc. Bull.*, 2000, **25**, 15.

7 W. E. Devaney, W. S. Chen, J. M. Stewart and R. A. Mickelsen, *IEEE Trans. Electron Devices*, 1990, **37**, 428.

8 X. Zhu, I. Yuri, X. Gan, I. Suzuki and G. Li, *Biosens. Bioelectron.*, 2007, **22**, 1600.

9 Z. Y. Fan and J. G. Lu, *Appl. Phys. Lett.*, 2005, **86**, 123510.

10 S. Kumar, V. Gupta and K. Sreenivas, *Nanotechnology*, 2005, **16**, 1167.

11 P.S. Drazic, Liquid Crystal Dispersion, World Scientific, Singapore, 1995.

12 J.W. Doane, A. Golemme, J.L. West, J.B. Whitehead, and B.G. Wu, Polymer dispersed liquid crystals for display application, Mol. Cryst. Liq. Cryst. 1988,**165**, 511.

13 P. Malik and K.K. Raina, *Physica B Cond. Matt.,* 2010, **405**, 161.

14 P. Malik and K.K. Raina, *Opt. Mat.* 2004, **27**, 613.

15 F. Zhang, X. Wang, S. Ai, Z. Sun, Q. Wan, Z. Zhu, Y. Xian, L. Jin and K. Yamamoto, *Anal. Chim. Acta*, 2004, **519**, 155.

16 X. Fan, M. L. Zhang, I. Shafiq, W. J. Zhang, C. S. Lee and S. T. Lee, *Adv. Mater.*, 2009, **21**, 2393.

17 S. Chandrasekhar, *Liquid Crystals*, Cambridge University Press: 1977, Cambridge, London.

18 K. Pal, U. N. Maiti, T. P. Majumder, S. C. Debath, S. Ghosh, S. K. Roy, N. Bennis and J. M. Otón, *Nanotechnology*, 2013, **24,** 125702.

19 T. Kato and J. M. J. Frechet, *Macromol. Symp.*, 1995, **98**, 311.

20 C. M. Paleos and D. Tsiourvas, *Angew. Chem., Int. Ed. Engl.*, 1995, **34**, 1696.

21 T. Kato and J. M. J. Frechet, *J. Am. Chem. Soc.*, 1989, **111**, 8533.

22 T. Kato, A. Fujishima and J. M. J. Frechet, *Chem. Lett.*, 1990, **19**, 919.

23 T. Kato, J. M. J. Frechet, P. G. Wilson, T. Saito, T. Uryu, A. Fujishima, C. Jin and F.

Kaneuchi, *Chem.Mater.*, 1993, **5**, 1094.

24 T. Kato, H. Kihara, U. Kumar, T. Uryu and J. M. J. Frechet, *Angew. Chem., Int. Ed.Engl.*, 1994, **33**, 1644.

25 T. Kato, M. Fukumasa and J. M. J. Frechet, *Chem. Mater.* 1995, **7**, 368.

26 T. Kato, T. Nakano, M. Moteki and T. Uryu, *Macromolecules*, 1995, **28**, 8875.

27 T. Kato, Y. Kubota, M. Nakano and T. Uryu, *Chem. Lett.*, 1995, **161**, 1127.

28 W. S. Koo, H. K. Chung, H. G. Park, J. J. Han, H. C. Jeong, M. J. Cho, D. H. Kim and D. S. Seo, *J. Nanosci Nanotechnol.* 2014 ,**14**,8609.

29 R. K. Shukla, C. M. Liebig, D. R. Evansb and W. Haase, *RSC Adv.*, 2014,**4**, 18529.

30 A. Chaudhary, P. Malik, R. Mehra, and K.K. Raina, *Phase Transitions.* 2012, **85**, 244.

31 P. K. Tripathi, A. K. Misra, K. K. Pandey, S. P. Yadav and R. Manohar, *Phase Transitions: A Multinational Journal*, 2013, **86**, 1241.

32 Khushboob, D. Jayoti, P. Malik, A. K. Chaudhary, R. Mehraa and K. K. Raina, *Integrated Ferroelectrics: An International Journal*, 2014, **158**, 123.

33. P. Nayek and G. Li, Scientific Reports, 2015, **5**, 10845.

33 S. Osaki, S. Uemura and Y. Ishida, *Journal of Polymer Science*, 1974, **12,** 1727.

34 S. Murakami and H. Naito, *Japanese Journal of Applied Physics,* 1997, **36,** 2222.

35 P. Nayek, S. Ghosh, S. Karan, T. P. Majumder and S. K. Roy, *Appl. Phys. Lett.,* 2008, **93,** 112905.

36 S. Ghosh, P. Nayek, S. K. Roy, R. Gangopadhyay, M. R. Molla and R. Dabrowski, *Appl. Phys. Lett.,* 2010, **96,** 073101

37 G. Pandey, R. Dhar, V.K. Agrawal and R. Dabrowski, *Phase Trans.* 2004,**77**,1111.

38 K. Nakamoto, In Infrared and Raman Spectra of Inorganic and Co-ordination Compounds, Interscience: New York,(1978).

39 D. L. Pavia, G .M. Lampman and G .S. Kriz, Introduction to spectroscopy, Thomson Learning inc.: India (2007).

40 V. N. Vijayakumar and MLN Madhu Mohan, *Sol. State. Comm.*, 2009, **149**, 2090. Federal Republic of Germany.

Figures:

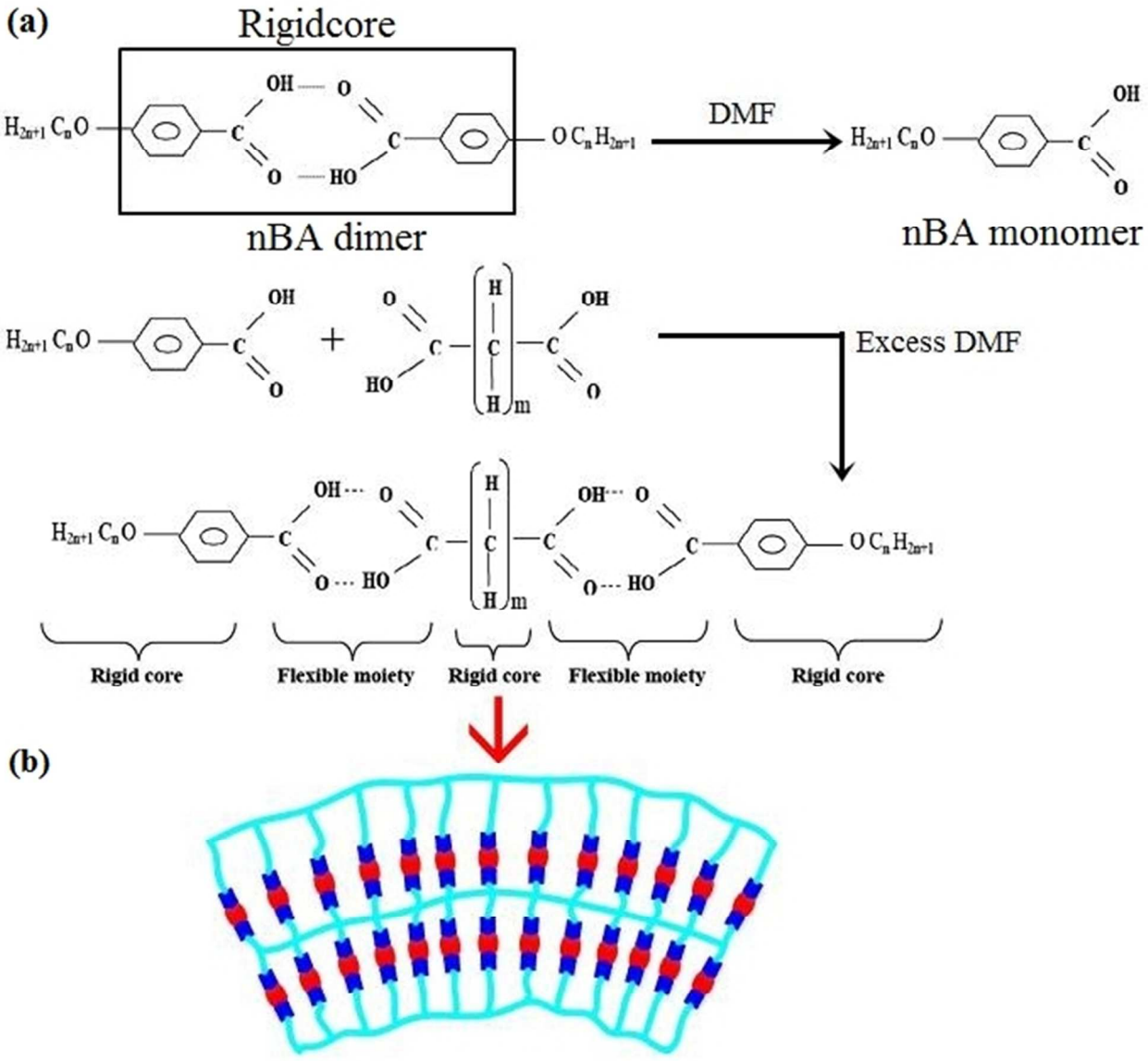

Figure1.(a) Molecular structure representation of rigid and flexible parts of azelatic acid with p-n heptyloxy benzoic acid hydrogen bonded liquid crystals complex (AC+nBAO, for n=7 and m=7 for AC), **(b)** schematic representations of corresponding HBLC structure.

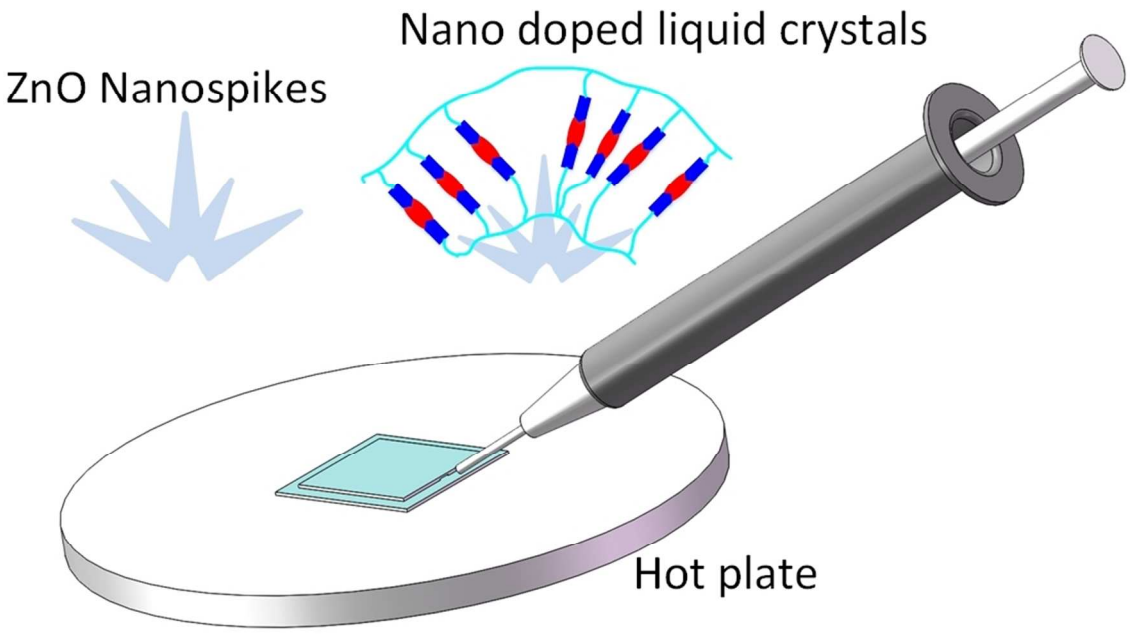

Figure2. Schematic representation of ZnO nanospikes dispersed hydrogen bonded liquid crystals sample distribution techniques into two electrode system sandwiched ITO cells.

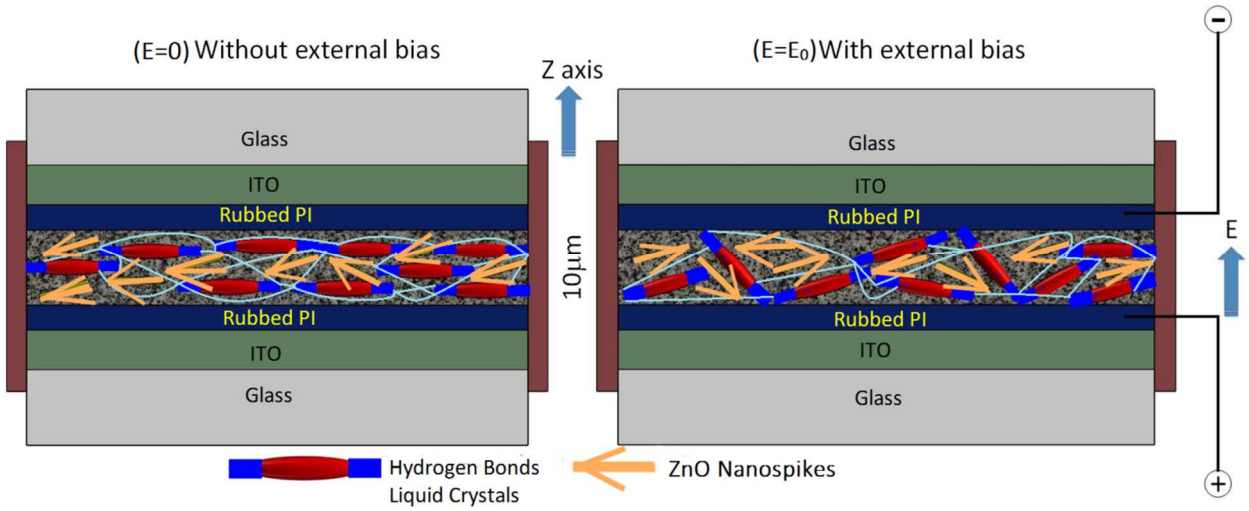

Figure3. Schematic of the side-view structure of the LC cell, internal device mechanism of hydrogen bonded liquid crystals and ZnO-nanospikes liquid crystals switching operation with and without an applying external bias. Note that the applied electric field is normal to the cell plane.

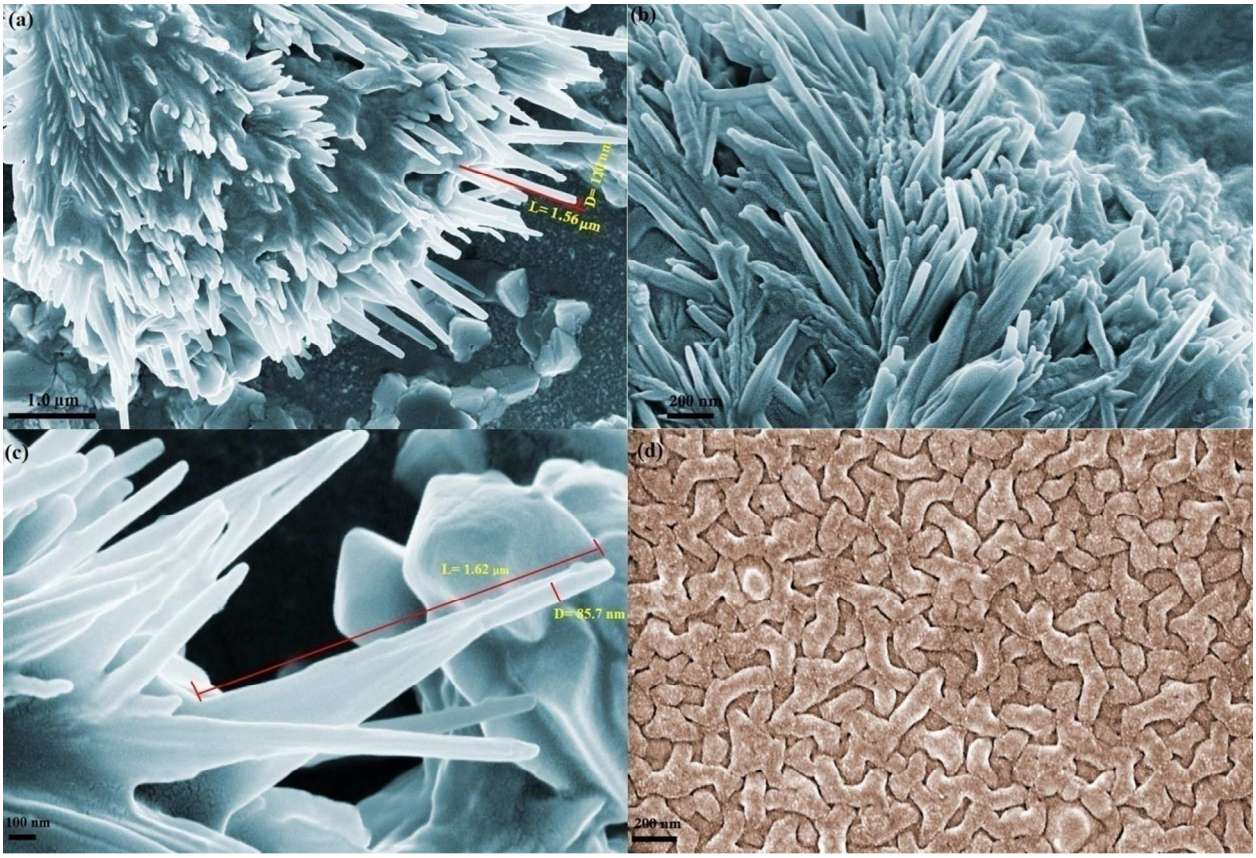

Figure4. FE-SEM images of uniform ZnO-nanospikes **(a)**1µm (low magnification), **(b)** 200nm (high magnification)**(c)**100nm, (very high magnification), in hydro-thermal route, and **(d)**ultrasonic vibration hydrogen bonded liquid crystals (azelaic acid with p-n heptyloxy benzoic acid) structures obtained at 200 nm (high magnification)

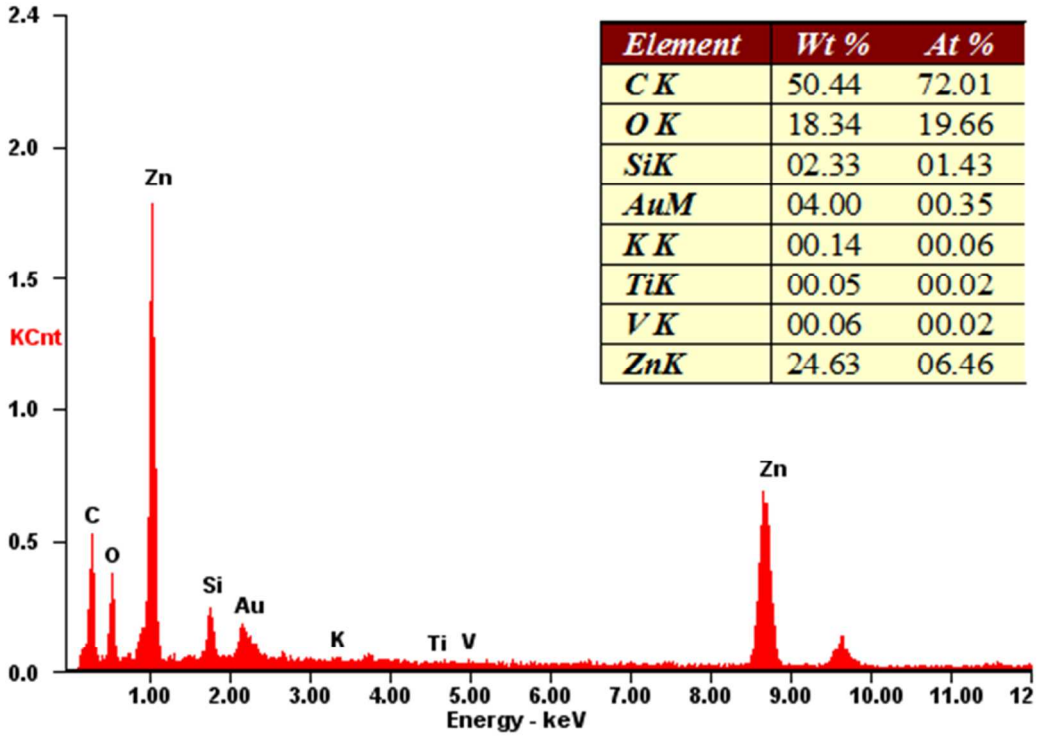

Element	Wt %	At %
C K	50.44	72.01
O K	18.34	19.66
SiK	02.33	01.43
AuM	04.00	00.35
K K	00.14	00.06
TiK	00.05	00.02
V K	00.06	00.02
ZnK	24.63	06.46

Figure5. EDS profile for the distribution of chemical elements inside ZnO-nanospikes encapsulated liquid crystals complex materials

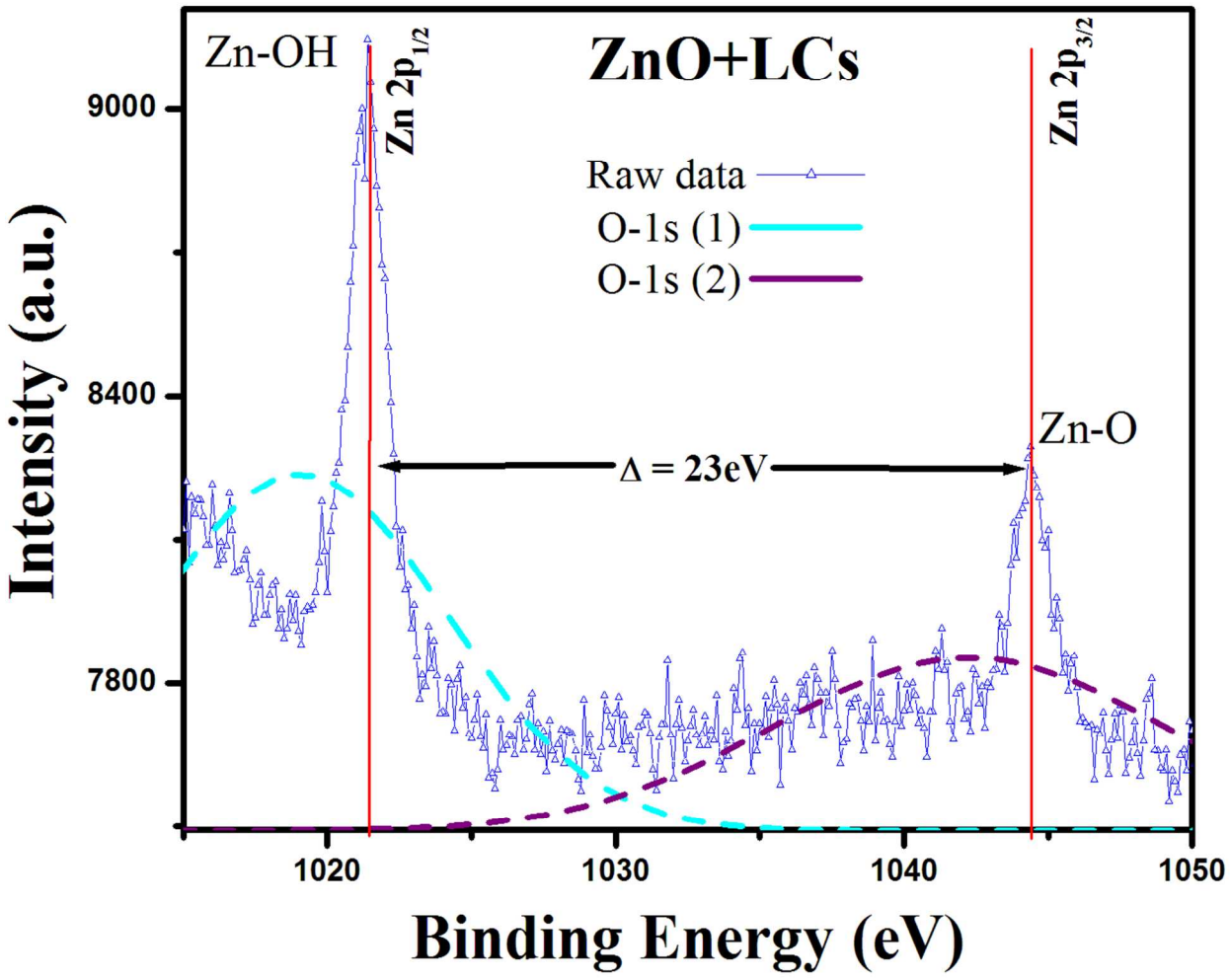

Figure6.XPS spectra of raw data of Zn $2p_{1/2,}$ $2p_{3/2}$ and O 1s (1,2) of ZnO-nanospikes morphologies synthesized via hydro-thermal assisted aqueous solution methods.

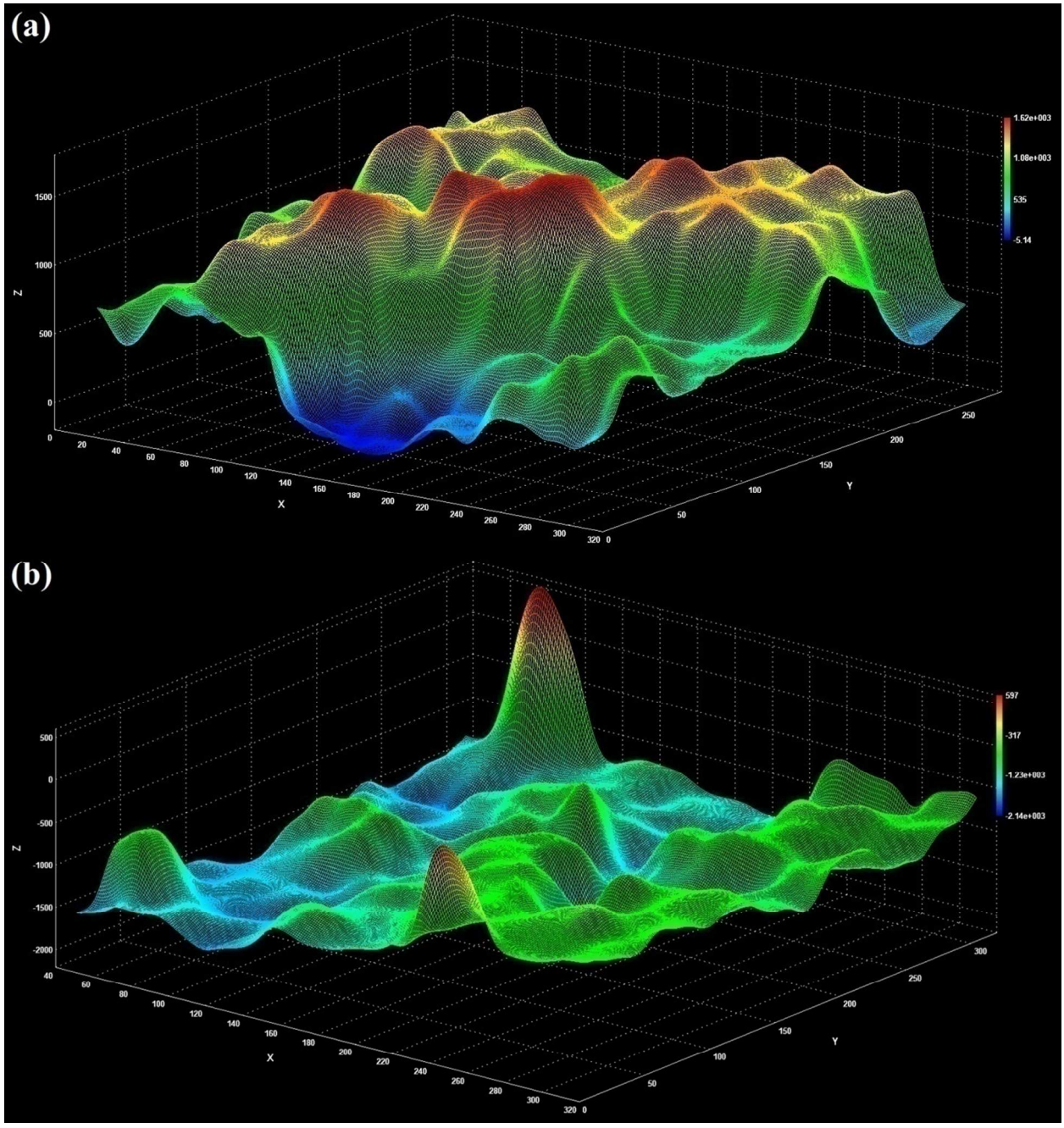

Figure7. Typical dark field image of scattering spectrum for cell shown in **(a)**general applied condition of ZnO-nanospikes dispersed liquid crystals cells **(b)** applied heating force for dark field interferometer includes a light source, detector, dark field optics and wavelength selection at either the illumination or detection section.

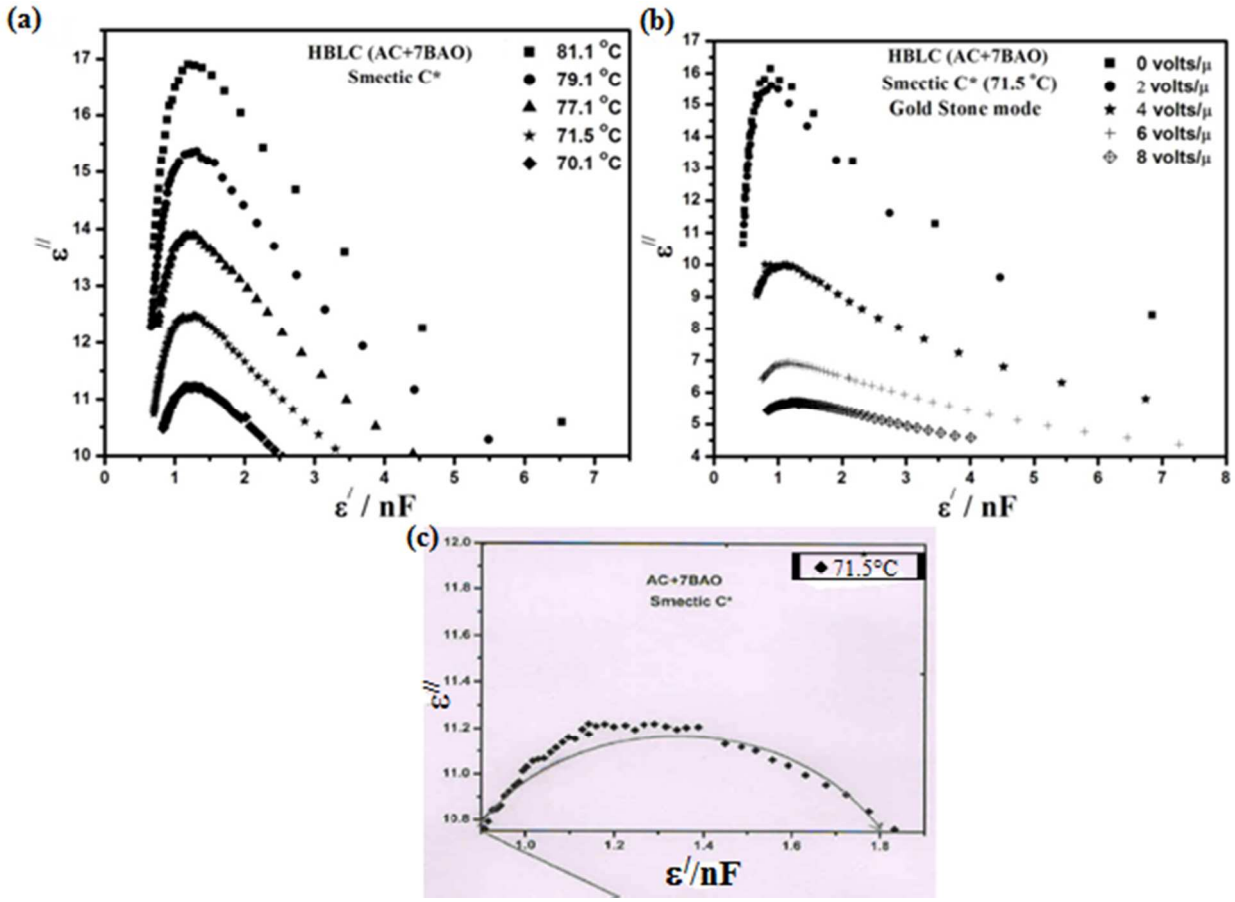

Figure8. (a) variation of relaxation frequency with temperature for Pure LC (AC+7BAO) in Gold stone model of smectic C* phase has been done at several temperatures e.g. 81.9^{o}C, 79.1^{o}C, 77.1^{o}C, 71.5^{o}C and 70.1^{o}C, **(b)** suppression of dielectric relaxation at different applied fields e.g. 0 V/μ, 2V/μ, 4V/μ, 6V/μ and 8V/μ the dielectric loss magnitude with permittivity is recorded at 77.1^{o}C, **(c)** The Cole-Davidson relaxation process at temperature 71.5°C.

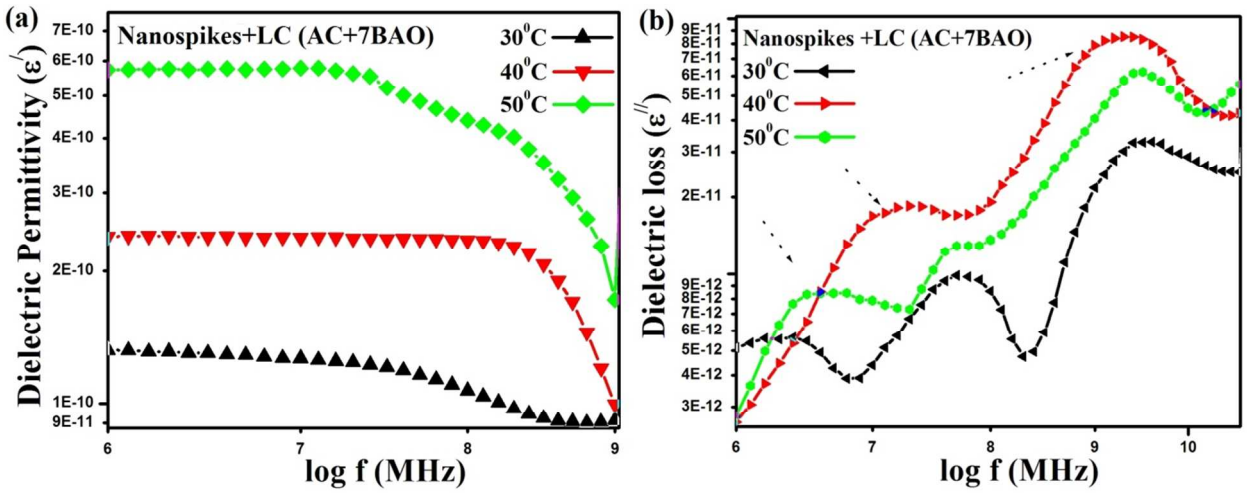

Figure9. Temperature dependence frequency dispersion dielectric response of ZnO-nanospikes dispersed liquid crystal sample **(a)** complex dielectric permittivity ($\varepsilon^{/}$), and **(b)** dielectric loss ($\varepsilon^{//}$) spectra, respectively.

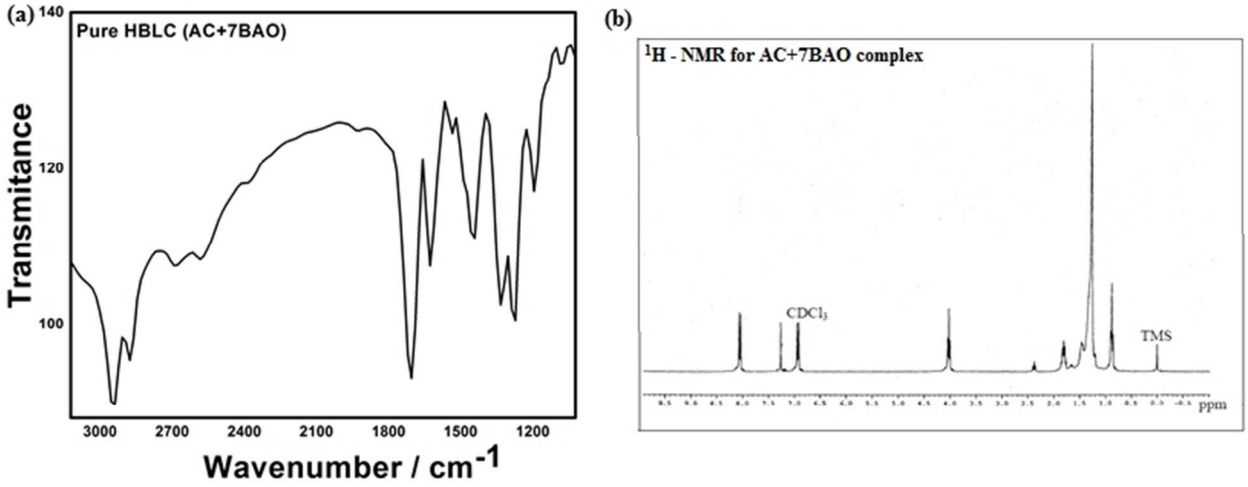

Figure10. (a) FTIR spectra and **(b)** ^{1}H NMR, for liquid crystals (AC+7BAO) complex

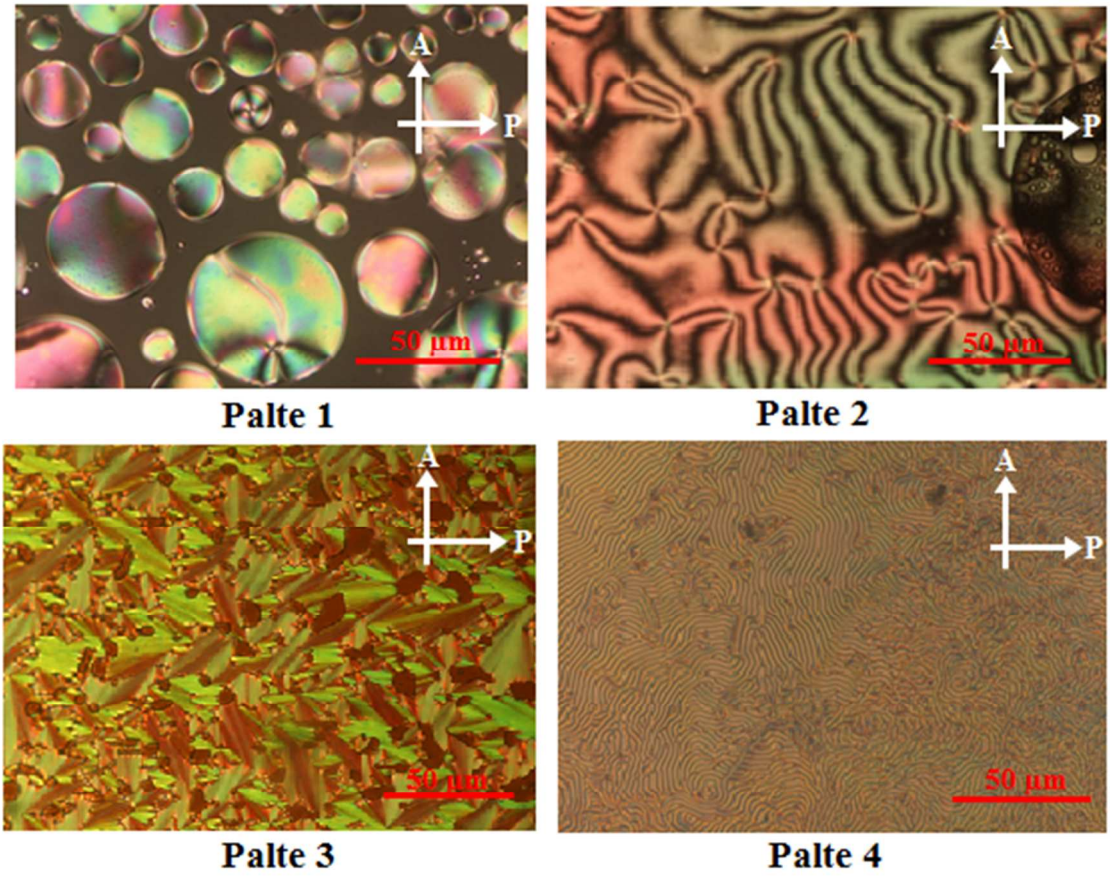

Figure11. A collection of optical micrograph under cross polarizer with 10x magnification corresponding to pure hydrogen bonded liquid crystals (AC+7BAO); nematic (N) droplet texture at 113.2°C (Plate 1), threaded nematic schlieren texture (Plate 2), smectic C* broken focal conic texture at 71.5°C (Plate 3) and smectic X* worm like texture at 81.9°C (Plate 4)

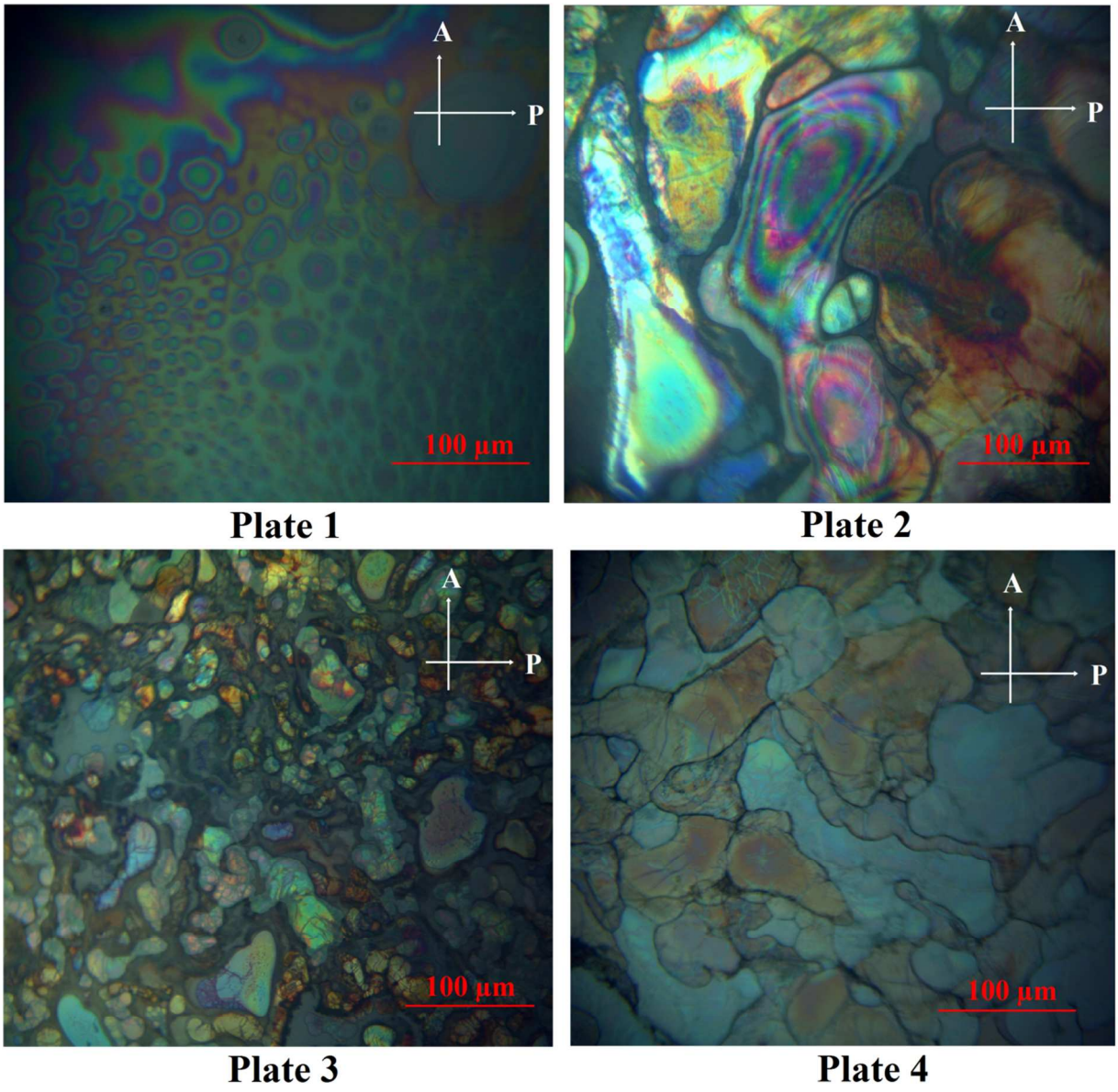

Figure12. A collection of texture studies optical micrograph under cross polarizer with 10x magnification of ZnO-nanospikes embedded liquid crystals; nematic (N) droplet texture at 113°C (Plate1), threaded nematic oily texture (Plate2), smectic C* mosaic texture pattern at 71.2°C (Plate 3), smectic X* cumulate texture at 81°C (Plate 4)

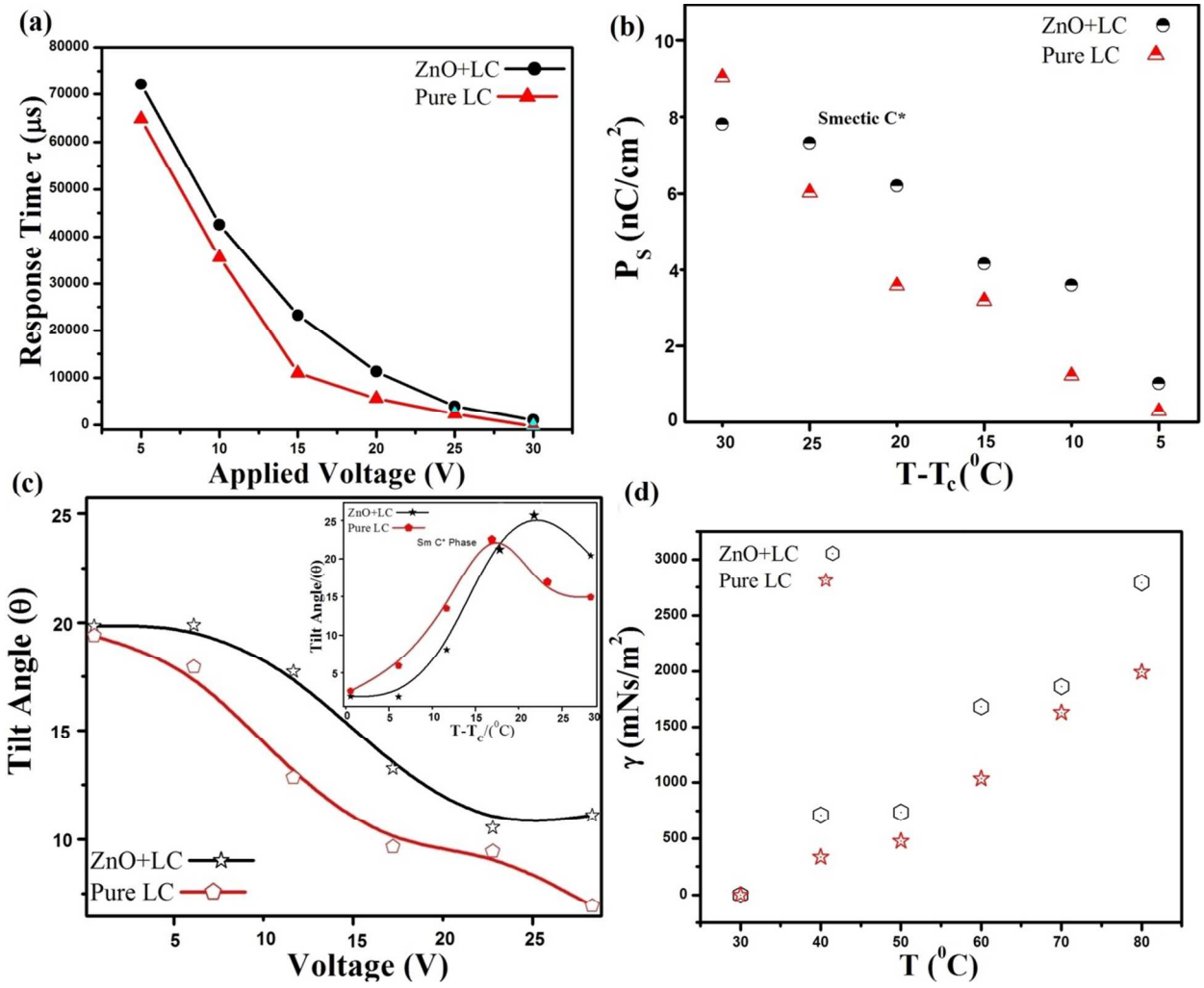

Figure13. Applied voltage and temperature dependence **(a)** electrical response time (τ), **(b)** spontaneous polarization (P_s) vs. phase transition, **(c)** field dependence optical tilt angle (θ) vs. applied voltage (V), (Inset: Tilt angle vs. phase transition in Smectic C* phase for homologous series (AC+7BAO) LC and nanospikes doped LC, and **(d)** rotational viscosity corresponding to pure liquid crystals and nanospikes dispersed liquid crystalline materials.

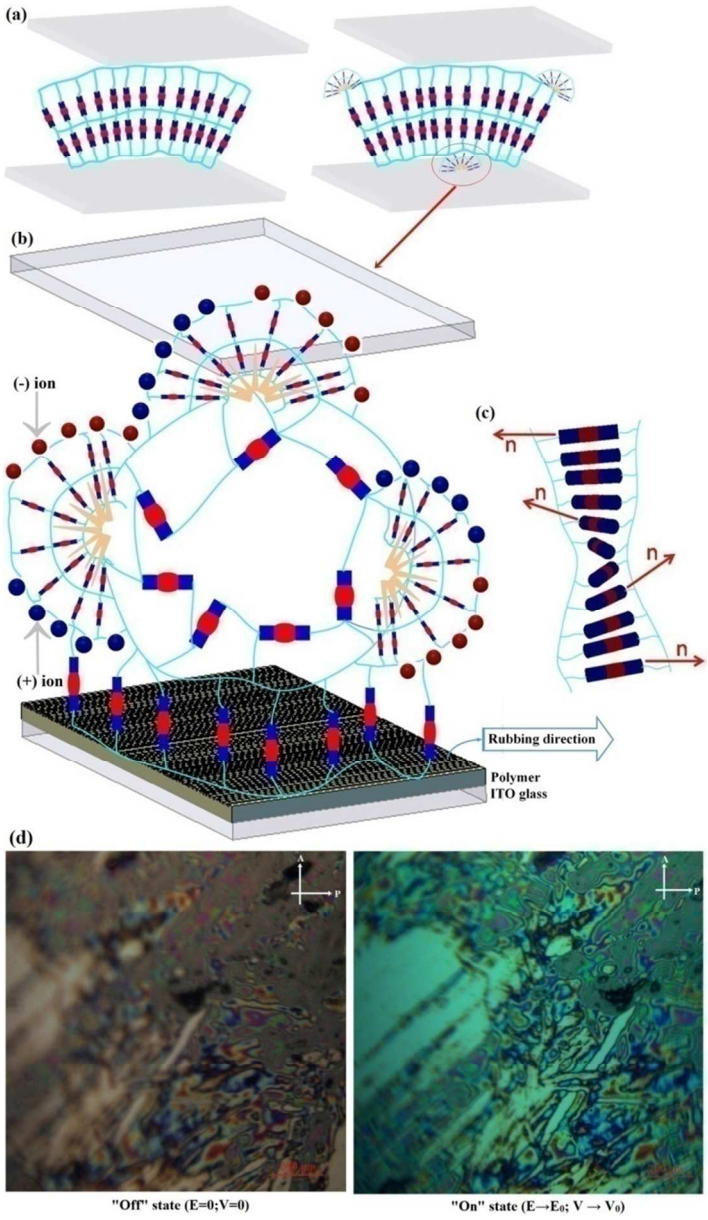

Figure14. (a) Schematic representation of a conventional pure LC cell and a NDLC cell constructed with the doped nanospikes**(b)** molecular orientation of hydrogen bonded liquid crystals and ZnO-nanospikes doped liquid crystals sandwiched two ITO cells **(c)** direction of polarization of HBLC molecules under cross polarizer **(d)** Microscopic investigation of the NDLC composite on the surface mechanism responsible for the high resolution switching performance (‘On state’ and ‘Off sate’) external bias field dependence in display device.

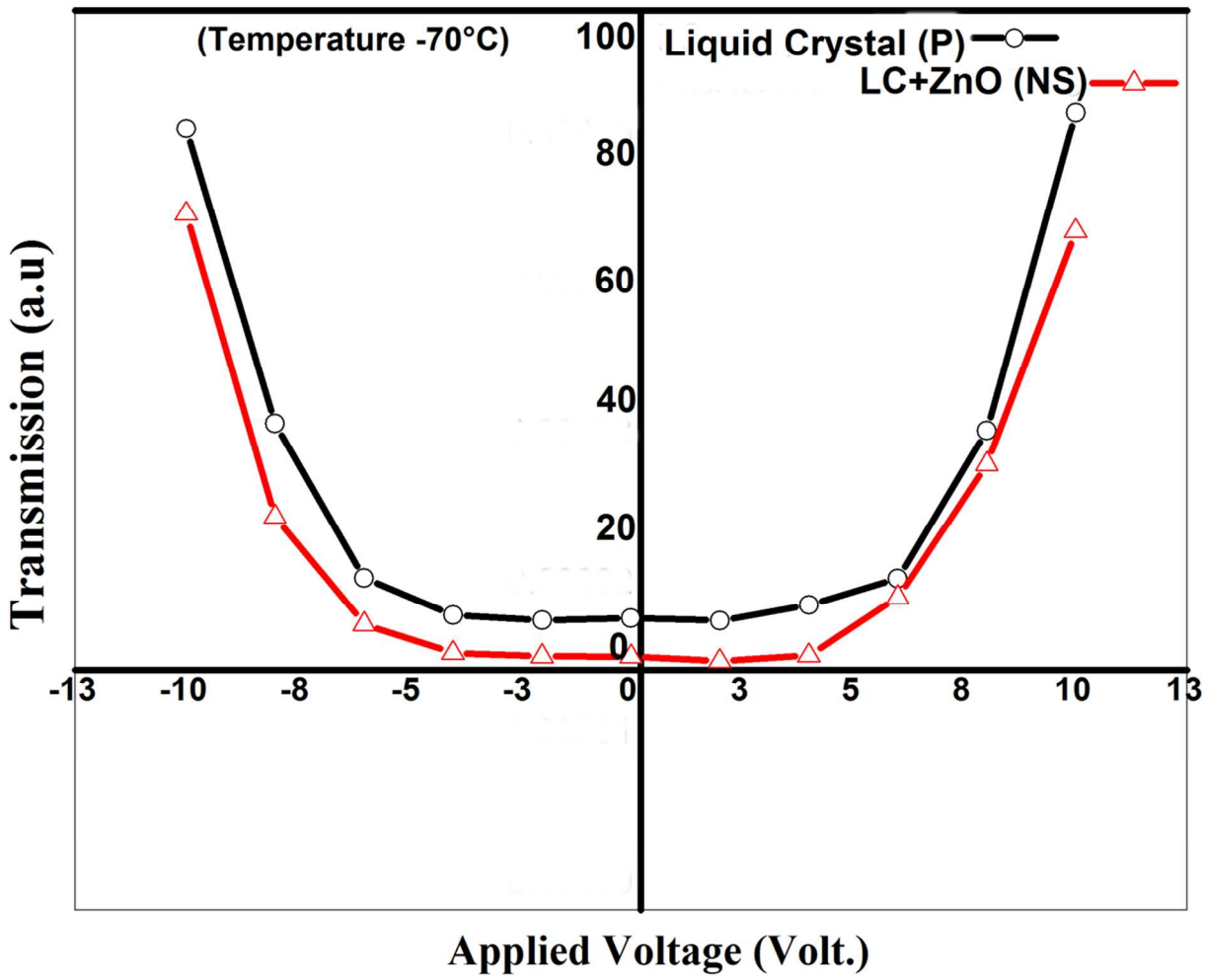

Figure15. Electro-optical transmittance vs. voltage characteristics of U-shape switching corresponds to pure LC and ZnO-nanospikes doped LC cells at 70°C.

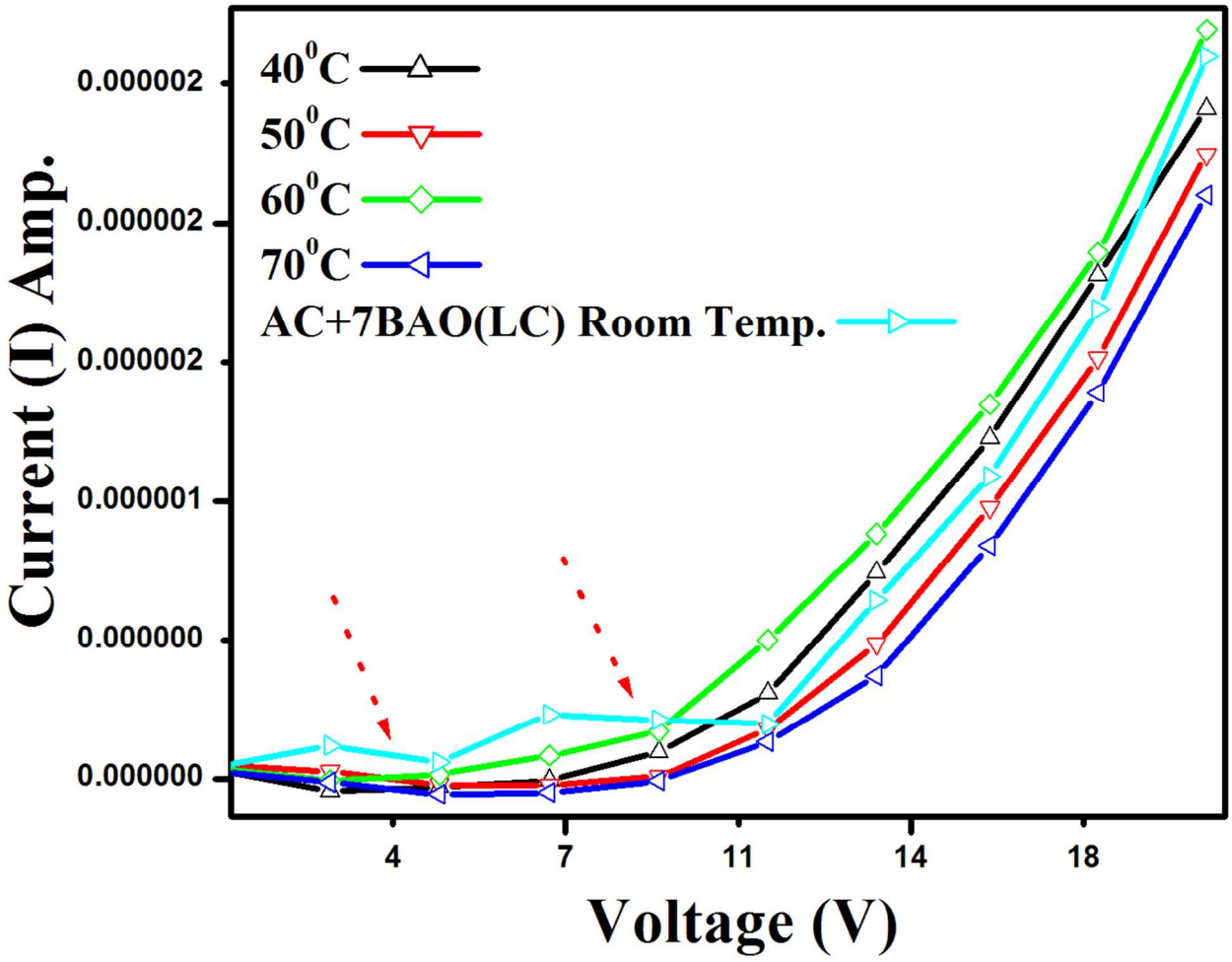

Figure16. Bistable DC switching of pure LC (room temperature) and temperature dependence I~V response characteristics of NDLC materials

Graphical Abstract